The International Journal of Advanced Manufacturing Technology (2023) 126:1233–1245
https://doi.org/10.1007/s00170-023-11202-w

ORIGINAL ARTICLE

# Compressive response versus power consumption of acrylonitrile butadiene styrene in material extrusion additive manufacturing: the impact of seven critical control parameters

**Markos Petousis[1] · Nectarios Vidakis[1] · Nikolaos Mountakis[1] · Emmanuel Karapidakis[2] · Amalia Moutsopoulou[1]**

Received: 22 December 2022 / Accepted: 1 March 2023 / Published online: 8 March 2023


## Abstract

Acrylonitrile butadiene styrene (ABS) is a multipurpose thermoplastic and the second most popular material in material extrusion (MEX) additive manufacturing (AM). It is widely used in various types of industrial applications in the automotive sector, housing, and food processing, among others. This work investigates the effect of seven generic control parameters (orientation angle, raster deposition angle, infill density, layer thickness, nozzle temperature, printing speed, and bed temperature) on the performance and the energy consumption of 3D-printed ABS parts in compression loading. Raw material with melt extrusion was formed in a filament form for MEX 3D printing. Samples after the ASTM D695-02a standard were 3D printed, with the seven control parameters, three levels, and five replicas each (135 experiments in total). Results were analyzed with statistical modeling tools regarding the compressive and the energy consumption metrics (printing time, weight, energy printing consumption/EPC, specific printing energy/SPE, specific printing power/SPP, compression strength, compression modulus of elasticity, and toughness). The layer thickness was the most critical control parameter. Nozzle temperature and raster deposition angle were the less critical parameters. This work provides reliable information with great technological and industrial impact.

**Keywords** Fused filament fabrication (FFF) · Material extrusion (MEX) · Optimization · Acrylonitrile butadiene styrene (ABS) · Energy consumption

## Nomenclature

| | |
|---|---|
| 3DP | 3D printing |
| ABS | Acrylonitrile butadiene styrene |
| AM | Additive manufacturing |
| ANOVA | Analysis of variances |
| BT | Bed temperature |
| DF | Degrees of freedom |
| DOE | Design of experiment |
| DSC | Differential scanning calorimetry |
| E | Tensile modulus of elasticity |
| EPC | Energy printing consumption |
| FFF | Fused filament fabrication |
| ID | Infill density |
| LT | Layer thickness |
| MEP | Main effect plot |
| MEX | Material extrusion |
| NT | Nozzle temperature |
| ORA | Orientation angle |
| PA | Polyamide |
| PT | Printing time |
| PS | Printing speed |
| RDA | Raster deposition angle |
| RQRM | Reduced quadratic regression model |
| sB | Compression strength |
| SEM | Scanning electron microscopy |
| SPE | Specific printing energy |
| SPP | Specific printing power |

✉ Nectarios Vidakis
vidakis@hmu.gr

Markos Petousis
markospetousis@hmu.gr

Nikolaos Mountakis
mountakis@hmu.gr

Emmanuel Karapidakis
karapidakis@hmu.gr

Amalia Moutsopoulou
amalia@hmu.gr

[1] Hellenic Mediterranean University, 71410 Heraklion, Greece

[2] Electrical and Computer Engineering Department, Hellenic Mediterranean University, 71410 Heraklion, Greece

Tg Glass transition temperature
TGA Thermogravimetric analysis

## 1 Introduction

Composites, due to their wide field of applications, have been thoroughly studied for their mechanical properties [1–4]. ABS is an engineering thermoplastic used in household equipment, electric and electronic devices [5, 6], automobile parts [7], and membranes [8]. Composites (carbon based [5, 6, 9], or others) have been developed to enhance ABS performance for specific applications. In MEX 3DP, ABS is the second most used polymer [10]. Therefore, research on its performance in AM is extensive, with the ABS polymer tested in pure form or as a matrix material in composites [11–19]. Its mechanical properties have been studied for tensile [20–25], flexural [22, 26, 27], creep [28], fatigue [29–33], dynamic loading [34], failure analysis [35], and impact tests [36–39]. The response of the ABS polymer in MEX 3D printing under different strain rates in the tensile test has also been reported [40, 41]. The effect of the 3D printing settings on the quality (surface roughness, dimensional accuracy, and porosity) of the parts built with the MEX process has been investigated, with the experimental results analyzed with statistical modeling tools [42–46]. The response of the ABS polymer in MEX 3D printing after successive recycling processes has been reported, showing that the material can withstand up to six repetitions of the process without serious compromise of its mechanical properties [47–50]. It has also been used in hybrid AM processes (AM with laser cutting for surface quality improvement [51], injection molding [52], shot peening [53], rotary friction welding [31], and friction stir welding for manufacturing of large parts [54]) to further expand its fields of application.

The effect of the 3DP parameters on the compression performance has been studied, focusing mainly on a limited number of parameters (one to three) [48, 55–66]. Still, research indicates the importance of compressive loading and how 3D-printed parts behave under such loading [67]. Modeling tools have been employed to analyze and optimize the studies' results [18, 68–70]. Such an approach is also applied for the investigation of the effect of the process parameters on the mechanical properties of MEX-printed parts for other polymeric materials as well [71, 72], indicating that this is a common and reliable approach.

Apart from the mechanical performance, a critical aspect of 3DP is the energy consumption due to its environmental effect [73–75]. For the assessment of this critical parameter in 3DP, models have been presented [73, 76] based on machine learning [75], life cycle analysis [74], and statistical modeling tools [10]. A very limited number of works are focusing on the energy consumption of the ABS material when 3DP and the effect of the 3D printing parameters [10, 77]. Most works either provide a holistic approach or study a limited number of parameters.

This work introduces for the first time inclusive compressive test results for ABS 3DP, which are now missing in the literature. Additionally, it thoroughly studies the effect of 3DP parameters on the energy performance of the MEX process. Energy performance and sustainability of manufacturing processes are nowadays hot issues with industrial and social interest. ABS was chosen to be studied, as it is the second most popular thermoplastic in MEX AM [47] and it is a popular material for different types of applications as mentioned above. A thorough study, considering simultaneously such a high number (seven) of 3D printing settings, on the response in compressive loading of parts 3D printed with the ABS thermoplastic is missing from the literature. For the energy consumption in MEX 3D printing, literature is still marginal, although it affects sustainability [76], which is a key aspect nowadays for AM technology [78, 79].

Seven control parameters (ORA, RDA, ID, LT, NT, PS, and BT) are studied herein, with three levels each. All are generic parameters, i.e., they do not depend on the specific 3D printer used. The response parameters of the study are related to both the mechanical properties of the 3DP ABS parts under compression loading and the consumption of energy during the MEX process (PT, weight, EPC, SPE, SPP, sB, E, and toughness). For the analysis and the optimization of the experimental results, statistical modeling tools were used. This work provides a roadmap for the seven 3DP parameters studied. The results presented indicate which set of parameter values is better in achieving the expected outcome in each case according to the specifications set (better strength or more eco-friendly energy consumption).

## 2 Materials and methods

### 2.1 Preparation of the samples

Figure 1 shows snapshots from the sequence of the experimental processes implemented in the work. ABS was procured from INEOS Styrolution (Frankfurt, Germany). The grade was terluran hi-10,and it has the following properties: $B$ 38 MPa, $E$ 1900 MPa, and density 1030 kg/m$^3$ (https://www.ineos-styrolution.com/Product/Terluran_Terluran-HI-10_SKU300600120831_lang_en_GB.html, accessed 01/12/2022). It was sourced in powder form. It was dried at 80 °C for 2 h following the manufacturer's specification, and then it was formed into a 1.75-mm diameter filament compatible with the MEX 3DP process (3devo precision, Utrecht, the Netherlands, nozzle 220 °C, mid chamber 230 °C, hopper 240 °C, 3.5 rpm, and 55% fan speed). The filament diameter was monitored

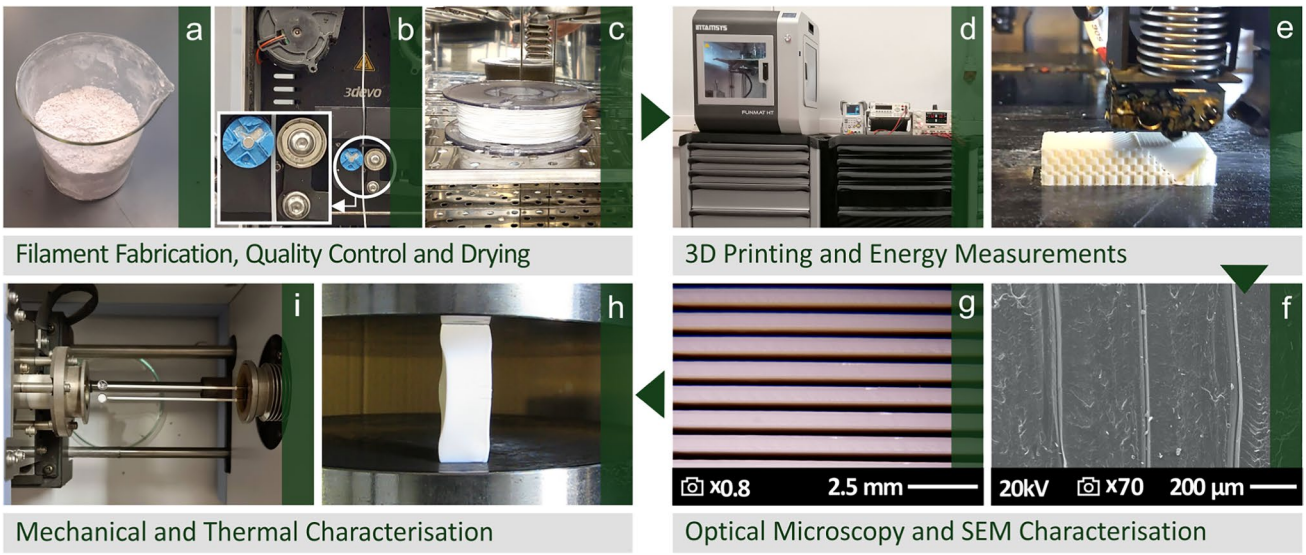


**Fig. 1** Successive experimental steps followed in the work

with the built-in sensor of the 3devo extruder, which operates in a closed-loop and adjusts the extruding parameters to achieve as accurate a diameter as possible during the process.

After a repetition of the drying process, compression samples were 3DP with various control parameter values. The 3D-printing settings used are shown in Fig. 2, and they are determined according to the literature review and preliminary tests. Five replicas were manufactured per case. An Intamsys Funmat HT (Shanghai, China) 3D printer was used, and the required G-code for the 3D printing process was prepared on the Intamsuite (Shanghai, China) software tool. Specimens were manufactured following the ASTM D695-02a international standard (samples of $50.8 \times 12.7 \times 12.7$ mm$^3$, Fig. 2). Specimens were manufactured for each set of 3D printing parameters in five replicas.

## 2.2 Energy consumption and metrics

Specimens were weighted in a high-accuracy electronic weight, while the consumed energy during the MEX 3DP process was recorded (Rigol DM3058E). The voltage (V) was considered constant during the process. It was measured at the beginning and the end of the 3D printing process to verify the statement. The electrical amplitude (A) was recorded during the 3D printing of the parts (sampling of 20 measurements per second), along with the elapsed time (stopwatch method [80]). From these measurements, the consumed energy was calculated in kWh and then converted to MJ for the determination of the EPC. The consumption

| 3D Printing Control Parameters | Value | Units |
|---|---|---|
| Infill Density (ID) | 60-80-100 | % |
| Raster Deposition Angle (RDA) | 0-45-90 | Deg |
| Nozzle Temperature (NT) | 210-230-250 | °C |
| Printing Speed (PS) | 20-40-60 | mm/s |
| Layer Thickness (LT) | 0.1-0.2-0.3 | mm |
| Bed Temperature (BT) | 80-100-120 | °C |
| Orientation Angle (ORA) | 0-45-90 | Deg |
| Number of Perimeters | 2 | – |
| Top solid layers | 0 | – |
| Bottom solid layers | 0 | – |

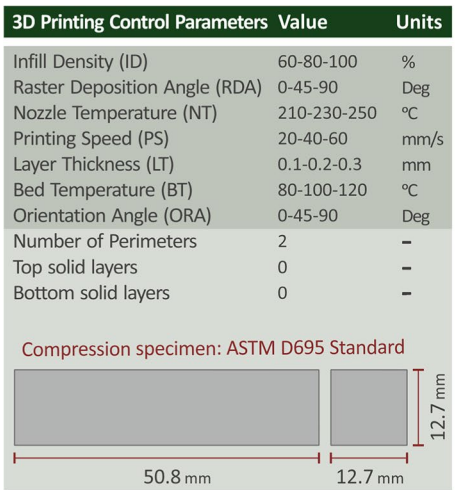


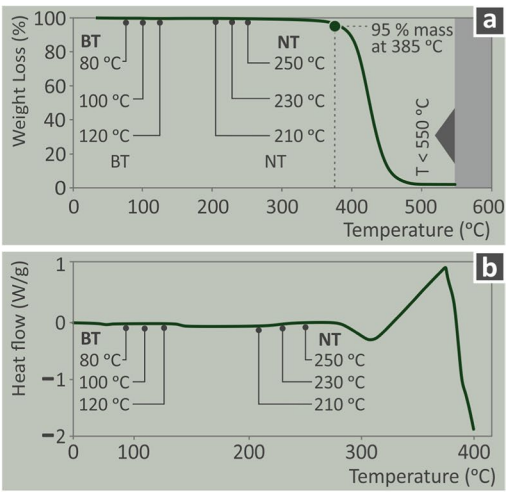


**Fig. 2** 3D-printing parameters used in the work and control parameter values. The geometry of the compression specimens is shown. **a** The material degradation graph, as acquired in the TGA, and **b** the graph acquired in the DSC (TGA and DSC: cycle 30 and 550 °C, step 10 °C/min)

of the energy is resolved in three (3) distinct stages: (*a*) 3D printer start-up, (*b*) 3D printing process, and (*c*) 3D printer shutdown, and can be yielded by:

$$E_{\text{total}} = E_{\text{thermal}} + E_{\text{motion}} + E_{\text{auxiliary}} \quad (1)$$

where

$$E_{\text{thermal}} = E_{\text{heating}} + E_{\text{cooling}} \quad (2)$$

$E_{\text{motion}}$ is the absorbed energy by the motors of the machine, whereas:

$$E_{\text{auxiliary}} = E_{\text{startup}} + E_{\text{steadystate}} + E_{\text{shutdown}} \quad (3)$$

Is the energy consumed by the 3D printer's electronics and other parts.

EPC, as it was recorded with the device, is the energy consumed from the beginning to the end of the MEX 3DP process. The energy required for the machine startup and shutdown is constant and independent of the material used for 3DP. The SPE index is calculated from the following equation (indicating the energy consumed per mass produced):

$$SPE = \frac{EPC}{w}\left[MJ/g\right] \quad (4)$$

where EPC represents the energy used by the 3D printer ($E_{\text{total}}$), and $w$ is the actual weight of each specimen.

The SPP index is calculated from the following equation (indicating the required power per mass produced):

$$SPP = \frac{EPC}{PT \times w} \bullet 10^3\left[\text{kW/g}\right] \quad (5)$$

where PT is the actual printing time for each experimental run.

To ensure that the temperatures used during the filament extrusion and the 3DP process were not affecting the thermal stability of the samples, TGA measurements were taken on the produced material, verifying this hypothesis (Fig. 2). DSC measurements were also taken to verify that the temperatures used in the work are not in areas in which the crystallinity of the material changes (Fig. 2).

### 2.3 Compression tests

Samples were tested for their compressive response on an Instron KN1200 (MA, USA) at 1.3 mm/min per the standard. Samples were examined for their morphological characteristics with optical microscopy (Kern OKO 1, with a 5MP type ODC 832 camera, Balingen, Germany) and a field emission SEM (Jeol JSM-IT700HR; Tokyo, Japan, Au sputtered samples, high vacuum mode, 20 kV acceleration voltage).

### 2.4 Design of experiment and ANOVA

Control parameters (ORA, degrees; RDA, degrees; ID, %; LT, mm; NT, °C; PS, mm/s; BT, °C) were selected according to the literature review, and they are satisfying two additional criteria to be generic, i.e., independent of the 3D printer used and to be continuous, i.e., without categorical control such as the infill pattern parameter, for example. Their levels were selected according to the literature [42, 43, 47], as well as the ABS material specs (NT, PS, and BT), and preliminary tests. A Taguchi $L_{27}$ array was compiled with five replicas each [81]. That is 135 experiments for the modeling process and the analysis of the compression strength results and the energy consumed for the 3DP of the samples. Full factorial modeling would require $5 \times 3^7$experimental runs. Results were validated with verification experiments. The five replicas per case evaluate the deviation in the experiments, the validation experiments, and the reliability of the results.

The response parameters were the PT (s) and $w$ (g), which are also used for the calculation of the energy-related outputs, i.e., EPC (in MJ), SPE (in MJ/g), and SPP (in KW/g). Compression strength response parameters were the sB (MPa), $E$ (MPa), and the toughness (MJ/m$^3$). Regression analysis evaluated the reliability of the modeling analysis and provided equations as functions of the process parameters for the prediction of the responses. The regression analysis is provided in the supplementary material of the study.

## 3 Results

### 3.1 Examination of the morphological characteristics of the samples

Figure 3 presents stereoscopic images from the top surface of randomly selected samples from different experimental runs. The differences in the 3DP parameters used in each different run, i.e., ORA, RDA, LT, and ID, can be easily distinguished in the images. In all images, a perfect 3DP structure is presented without defects or voids.

Figure 4a shows a graphical representation of the compression experiment, indicating how the 3DP structure is expected to behave and affects the results. Depending on the specimen's printed structure, shear failure begins as the specimen is subjected to a compressive load and gradually deforms. The specimen is subjected to the compressive load until it fully fails. The shattered surfaces are microscopy-inspected to investigate the failure mechanism. Figure 4b–e shows SEM images at 70 and × 300 from the fracture surface of two randomly selected samples built with ORA 45°, RDA 0°, LT 0.2 mm, and ID 100. The sample presented in Fig. 4b and c has been built with PS 20 mm/s, NT 230 °C, and BT 120 °C, while the sample presented in Fig. 4d and e has

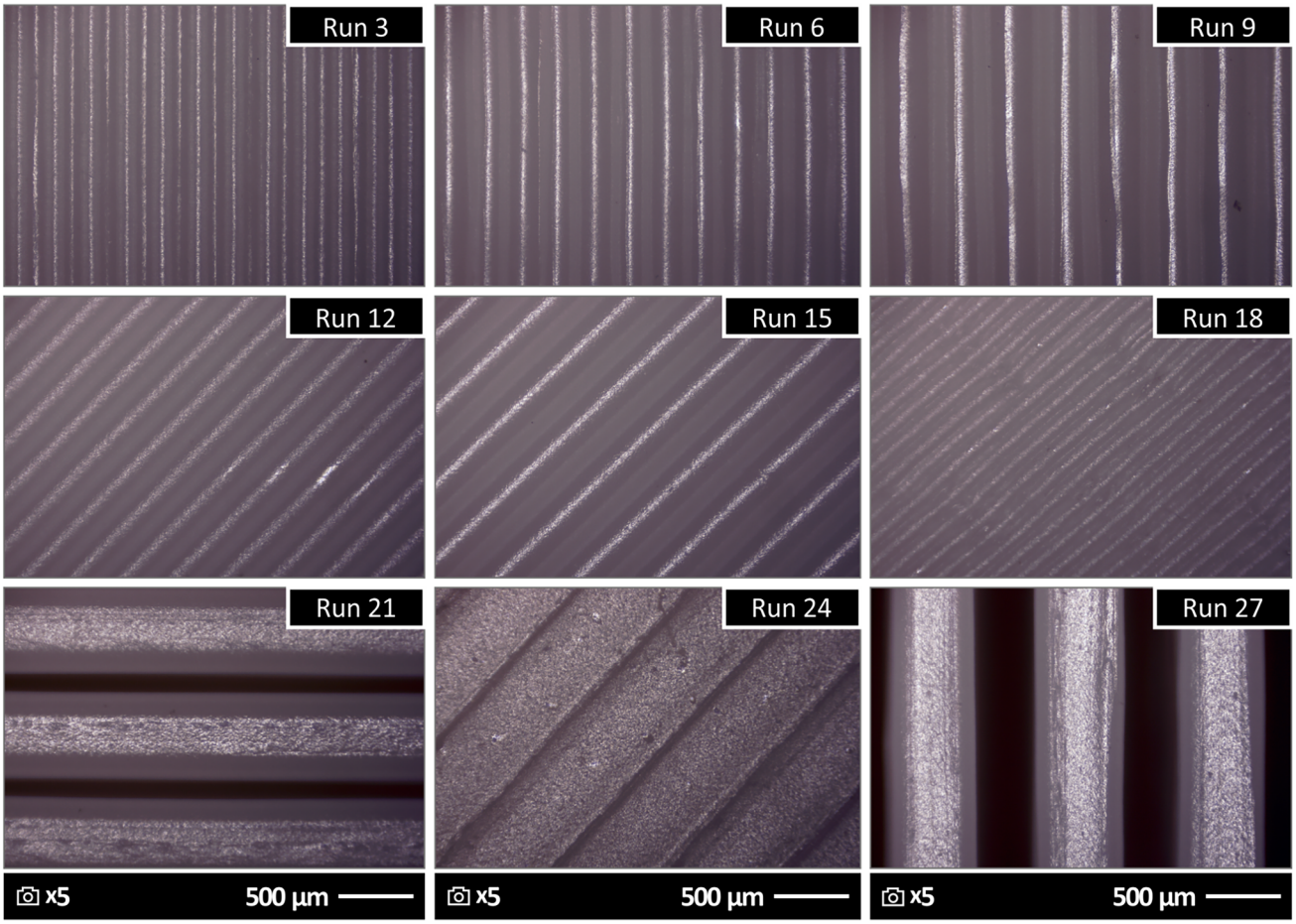


**Fig. 3** Typical 3D-printed samples with the various control parameters' values

been built with PS 40 mm/s, NT 250 °C, and BT 80 °C. The left sample shows higher deformation on the fracture surface than the right sample. The left sample has a more solid surface, while a crack has been formed in the fracture area of the right sample. In all cases studied, samples were fully fractured (divided into two pieces after the compression test) except for the case of samples built with ORA of 45°, in which the samples failed in the test without a full fracture occurring. It should be mentioned also that no buckling was observed in the samples during the tests.

### 3.2 Experimental results and statistical analysis

Table 1 presents the printing time (s) and weight (g) response parameter values with their deviation for the different control parameter levels. The corresponding MEPs that complied with the average response parameters' values are presented in Fig. 5. The two response parameters follow the same trend regarding the ORA, similar trends for the RDA, ID, NT, and BT, and different trends for LT and PS. RDA, LT, PS, NT, and BT do not significantly affect the weight of the 3DP parts, which is affected by the ORA and the ID control parameters. ORA of 0 and 90° reduces the weight, and 45° ORA increases it. The increase in the ID also increases the weight. Regarding the printing time, ORA of 0 and 90° reduces it, and 45° ORA increases it. A mild increase in the PT is presented, with an increase in the RDA. The increase in LT radically decreases the PT and is the number 1 ranked control parameter. The increase in the ID increases the PT, while, as expected, the increase in the PS reduces the PT, and PS is ranked as the no. 2 in importance of control parameters regarding the PT. NT and BT also have mild effects on the PT compared to other parameters and are ranked as the two least important control parameters for PT. The rank of all the control parameters for both PT and w is presented in Fig. 5. Table A in the supplementary data provides analytical results for each one of the experimental runs and replicas for the PT and weight response parameters.

Table 2 presents the mean average values with their deviation for the energy metrics and the compression mechanical properties related to response parameters per run. For the two main response parameters of EPC

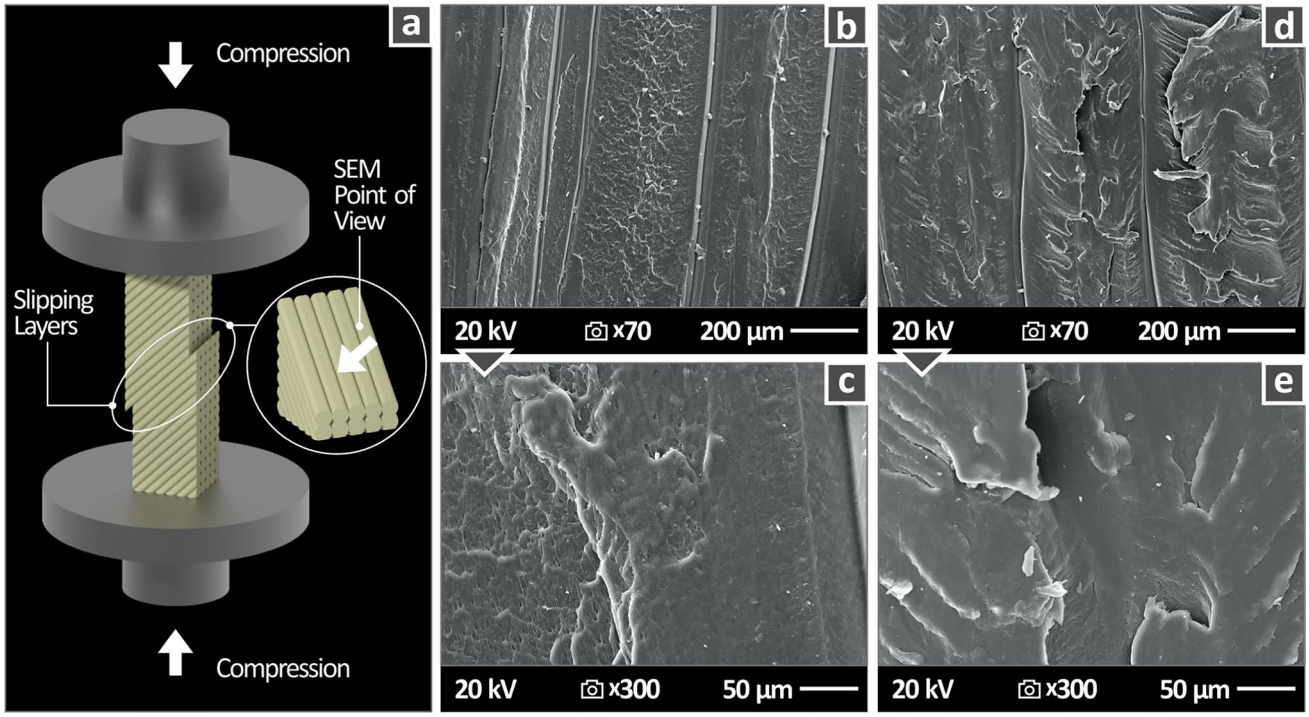


**Fig. 4** **a** Graphical representation of a 3D printed sample compression test, SEM images of the fracture surface of samples built with ORA 45°, RDA 0°, LT 0.2 mm, ID 100 and PS 20 mm/s, NT 230 °C, and BT 120 °C at a magnification of **b**×70 and **c**×300, and PS 40 mm/s, NT 250 °C, and BT 80 °C at a magnification of **d**×70 and **e**×300.

and sB, MEPs have been compiled and are presented in Fig. 6. From the produced graph, no clear relation between the compressive strength and the consumed energy can be derived. The two response parameters follow a similar trend only for the LT control parameters; still, in the sB, high values improve the optimization, while in the EPC, low values are better. Both response parameters are not significantly affected by the NT and BT control parameters. PS does not significantly affect the sB, while the increase in PS reduces EPC and is the rank 2 control parameter for the EPC; 0° ORA provides high sB values, with low EPC. The highest EPC with the lowest sB is observed at 45° ORA; 90° ORA gives better results than 45° ORA regarding the sB, with low EPC. The increase in RDA reduces sB, with a significant decrease presented at 90°. At the same time, the increase in RDA increases the EPC. The 0° RDA gives the highest sB value, with low EPC. EPC is drastically reduced with the increase in LT, while the increase in LT decreases sB. Finally, the increase in ID significantly increases sB. The lowest EPC is reported for low ID values, and it increases with the increase in ID while maintaining the same level of values at the highest ID studied. Table B in the supplementary data provides analytical results for each one of the experimental runs and replicas for the EPC, SPE, SPP, sB, E, and toughness response parameters.

To further analyze the process mechanism, interaction plots are formed for sB and EPC for the control parameters studied (Fig. 7). For sB, ORA acts synergistically with ID, PS, NT, and BT and antagonistically with RDA and LT. RDA acts synergistically with PS, NT, and BT and antagonistically with the remaining control parameters. LT acts synergistically with PS, NT, and BT. ID acts synergically with PS, NT, and BT. PS acts synergistically with ID, LT, RDA, and ORA. NT acts synergistically with ID, LT, RDA, and ORA. BT acts synergistically with ID, LT, RDA, and ORA. Regarding the EPC, mostly antagonistic relations can be observed. ORA, RDA, and LT act synergistically with LT, and RDA with PS, NT, and BT. ID acts synergistically with PS, NT with LT and RDA, and BT with LT. Figure 8 presents the sB and EPC response parameters as surface graphs for the control parameters with the highest ranks.

## 4 Discussion

Herein, the energy consumption, which is a critical parameter for the sustainability of a process, was quantified for 3D printing parts with the ABS polymer using the MEX process. At the same time, an attempt was made to optimize the mechanical properties of the 3D-printed parts under compression loading. It was not possible to optimize both

**Table 1** Taguchi L27 design: control parameters, levels, mean average values, and standard deviations of measured responses for printing time and specimen weight

| Run | ORA | RDA | LT | ID | PS | NT | BT | Printing time (s) | Weight (g) |
|---|---|---|---|---|---|---|---|---|---|
| 1 | 0 | 0 | 0.1 | 60 | 20 | 210 | 80 | 7600.60 ± 170.24 | 5.60 ± 0.20 |
| 2 | 0 | 0 | 0.1 | 60 | 40 | 230 | 100 | 4080.40 ± 129.00 | 5.76 ± 0.22 |
| 3 | 0 | 0 | 0.1 | 60 | 60 | 250 | 120 | 2915.40 ± 65.81 | 5.61 ± 0.21 |
| 4 | 0 | 45 | 0.2 | 80 | 20 | 210 | 80 | 4654.20 ± 137.26 | 7.42 ± 0.26 |
| 5 | 0 | 45 | 0.2 | 80 | 40 | 230 | 100 | 2558.80 ± 64.34 | 7.28 ± 0.06 |
| 6 | 0 | 45 | 0.2 | 80 | 60 | 250 | 120 | 1868.20 ± 72.63 | 7.31 ± 0.27 |
| 7 | 0 | 90 | 0.3 | 100 | 20 | 210 | 80 | 3607.60 ± 91.58 | 8.39 ± 0.25 |
| 8 | 0 | 90 | 0.3 | 100 | 40 | 230 | 100 | 1864.60 ± 55.68 | 8.33 ± 0.19 |
| 9 | 0 | 90 | 0.3 | 100 | 60 | 250 | 120 | 1353.00 ± 35.13 | 8.41 ± 0.32 |
| 10 | 45 | 0 | 0.2 | 100 | 20 | 230 | 120 | 7710.00 ± 247.21 | 12.41 ± 0.38 |
| 11 | 45 | 0 | 0.2 | 100 | 40 | 250 | 80 | 4191.20 ± 150.09 | 12.54 ± 0.41 |
| 12 | 45 | 0 | 0.2 | 100 | 60 | 210 | 100 | 3064.00 ± 86.49 | 12.54 ± 0.39 |
| 13 | 45 | 45 | 0.3 | 60 | 20 | 230 | 120 | 4112.00 ± 87.27 | 10.03 ± 0.30 |
| 14 | 45 | 45 | 0.3 | 60 | 40 | 250 | 80 | 2207.20 ± 35.94 | 9.78 ± 0.36 |
| 15 | 45 | 45 | 0.3 | 60 | 60 | 210 | 100 | 1657.20 ± 36.91 | 10.27 ± 0.27 |
| 16 | 45 | 90 | 0.1 | 80 | 20 | 230 | 120 | 13,749.80 ± 455.65 | 11.22 ± 0.13 |
| 17 | 45 | 90 | 0.1 | 80 | 40 | 250 | 80 | 7456.80 ± 309.02 | 11.34 ± 0.27 |
| 18 | 45 | 90 | 0.1 | 80 | 60 | 210 | 100 | 5514.40 ± 188.23 | 11.25 ± 0.44 |
| 19 | 90 | 0 | 0.3 | 80 | 20 | 250 | 100 | 2583.20 ± 73.76 | 6.44 ± 0.19 |
| 20 | 90 | 0 | 0.3 | 80 | 40 | 210 | 120 | 1334.60 ± 31.10 | 6.41 ± 0.20 |
| 21 | 90 | 0 | 0.3 | 80 | 60 | 230 | 80 | 899.60 ± 38.65 | 6.27 ± 0.16 |
| 22 | 90 | 45 | 0.1 | 100 | 20 | 250 | 100 | 9830.80 ± 247.57 | 8.49 ± 0.27 |
| 23 | 90 | 45 | 0.1 | 100 | 40 | 210 | 120 | 5328.80 ± 136.46 | 8.33 ± 0.26 |
| 24 | 90 | 45 | 0.1 | 100 | 60 | 230 | 80 | 3808.80 ± 97.27 | 8.37 ± 0.24 |
| 25 | 90 | 90 | 0.2 | 60 | 20 | 250 | 100 | 3477.20 ± 95.31 | 5.30 ± 0.15 |
| 26 | 90 | 90 | 0.2 | 60 | 40 | 210 | 120 | 1773.60 ± 39.14 | 5.36 ± 0.15 |
| 27 | 90 | 90 | 0.2 | 60 | 60 | 230 | 80 | 1257.40 ± 37.26 | 5.46 ± 0.09 |

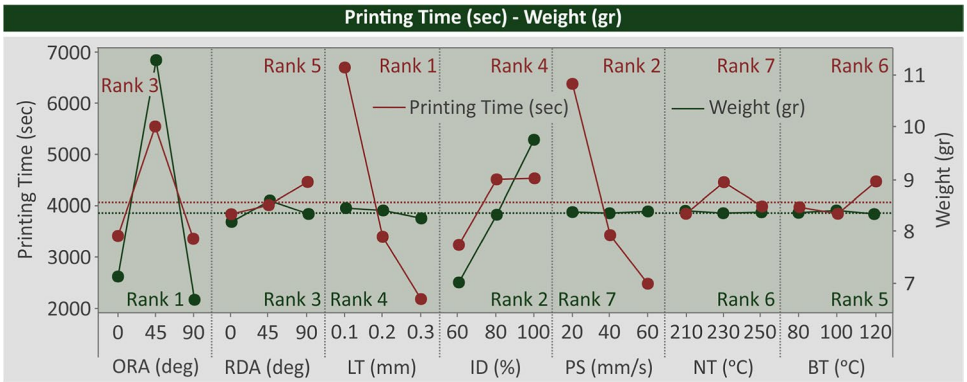


**Fig. 5** MEP of printing time (s) and weight (g) for the different control parameters

the energy consumption and the compressive strength simultaneously, employing one common set of 3D printing settings. Still, it was found that parts with improved mechanical strength can be built using moderate energy amounts. On the other hand, if energy consumption is the priority, it is possible to build parts with sufficient strength under compression loads, with reduced energy demands. Seven critical 3D printing parameters were studied, and it was found that the selection of appropriate 3D printing settings can significantly affect the performance of the built parts. For example, the compression strength of parts built with different values of the ORA setting can differ up to more than 40%, showing the significance of the 3D printing setting selection. The ID was the dominant parameter affecting the compressive strength of the parts, with the difference in the compressive strength of parts build with different ID exceeding 100%. So, selecting appropriate 3D settings is the first step toward the production of 3D-printed parts with

**Table 2** Mean average values and standard deviations of measured responses for EPC, SPE, SPP, compression strength, compression modulus of elasticity, and compression toughness

| Run | EPC (MJ) | SPE (MJ/g) | SPP (kW/g) | sB (MPa) | *E* (MPa) | Toughness (MJ/m$^3$) |
|---|---|---|---|---|---|---|
| 1 | 2.3 ± 0.1 | 0.41 ± 0.02 | 0.05 ± 0.00 | 46.7 ± 1.2 | 1056.5 ± 60.0 | 3.9 ± 0.4 |
| 2 | 1.3 ± 0.0 | 0.22 ± 0.01 | 0.05 ± 0.00 | 49.0 ± 0.5 | 1141.8 ± 12.8 | 4.5 ± 0.3 |
| 3 | 1.0 ± 0.0 | 0.18 ± 0.00 | 0.06 ± 0.00 | 48.7 ± 1.0 | 1126.4 ± 37.8 | 5.0 ± 0.2 |
| 4 | 1.4 ± 0.0 | 0.19 ± 0.01 | 0.04 ± 0.00 | 53.3 ± 0.9 | 1150.2 ± 45.1 | 7.7 ± 0.3 |
| 5 | 0.8 ± 0.0 | 0.11 ± 0.00 | 0.04 ± 0.00 | 55.6 ± 0.4 | 1132.5 ± 24.7 | 7.9 ± 0.1 |
| 6 | 0.7 ± 0.0 | 0.09 ± 0.00 | 0.05 ± 0.00 | 53.4 ± 0.7 | 1073.7 ± 37.7 | 7.8 ± 0.1 |
| 7 | 1.1 ± 0.0 | 0.13 ± 0.01 | 0.04 ± 0.00 | 59.8 ± 0.4 | 1115.3 ± 42.5 | 9.4 ± 0.1 |
| 8 | 0.6 ± 0.0 | 0.07 ± 0.00 | 0.04 ± 0.00 | 58.9 ± 0.7 | 1132.4 ± 13.2 | 9.6 ± 0.3 |
| 9 | 0.5 ± 0.0 | 0.06 ± 0.00 | 0.04 ± 0.00 | 51.0 ± 0.4 | 882.6 ± 103.9 | 8.4 ± 0.2 |
| 10 | 2.6 ± 0.1 | 0.21 ± 0.00 | 0.03 ± 0.00 | 52.7 ± 4.4 | 951.7 ± 49.5 | 2.8 ± 0.8 |
| 11 | 1.3 ± 0.0 | 0.10 ± 0.00 | 0.02 ± 0.00 | 51.0 ± 1.9 | 771.8 ± 142.3 | 7.1 ± 1.5 |
| 12 | 1.0 ± 0.0 | 0.08 ± 0.00 | 0.03 ± 0.00 | 53.0 ± 1.5 | 958.5 ± 124.5 | 5.7 ± 1.9 |
| 13 | 1.5 ± 0.1 | 0.14 ± 0.01 | 0.04 ± 0.00 | 17.8 ± 0.5 | 326.5 ± 61.1 | 3.0 ± 0.2 |
| 14 | 0.7 ± 0.0 | 0.07 ± 0.00 | 0.03 ± 0.00 | 22.0 ± 0.9 | 440.3 ± 28.5 | 3.8 ± 0.1 |
| 15 | 0.5 ± 0.0 | 0.05 ± 0.00 | 0.03 ± 0.00 | 23.6 ± 0.6 | 550.7 ± 66.6 | 3.6 ± 0.2 |
| 16 | 4.7 ± 0.1 | 0.42 ± 0.01 | 0.03 ± 0.00 | 25.0 ± 2.1 | 444.3 ± 98.6 | 3.8 ± 0.2 |
| 17 | 2.4 ± 0.1 | 0.21 ± 0.01 | 0.03 ± 0.00 | 28.2 ± 1.9 | 624.2 ± 14.8 | 4.4 ± 0.2 |
| 18 | 1.7 ± 0.0 | 0.15 ± 0.01 | 0.03 ± 0.00 | 30.4 ± 2.7 | 655.6 ± 34.7 | 4.4 ± 0.2 |
| 19 | 0.9 ± 0.0 | 0.13 ± 0.01 | 0.05 ± 0.00 | 39.8 ± 5.1 | 1037.0 ± 29.8 | 2.9 ± 0.9 |
| 20 | 0.4 ± 0.0 | 0.07 ± 0.00 | 0.05 ± 0.00 | 40.2 ± 6.2 | 973.3 ± 29.6 | 3.2 ± 0.7 |
| 21 | 0.3 ± 0.0 | 0.04 ± 0.00 | 0.05 ± 0.00 | 37.8 ± 2.9 | 962.7 ± 60.2 | 2.9 ± 0.7 |
| 22 | 3.3 ± 0.1 | 0.39 ± 0.01 | 0.04 ± 0.00 | 64.4 ± 3.5 | 1085.1 ± 114.4 | 10.5 ± 0.5 |
| 23 | 1.7 ± 0.0 | 0.21 ± 0.01 | 0.04 ± 0.00 | 62.1 ± 2.4 | 907.6 ± 98.4 | 10.0 ± 0.3 |
| 24 | 1.1 ± 0.0 | 0.14 ± 0.01 | 0.04 ± 0.00 | **65.3 ± 1.3** | 1234.4 ± 54.0 | 10.0 ± 0.2 |
| 25 | 1.1 ± 0.0 | 0.21 ± 0.01 | 0.06 ± 0.00 | 14.0 ± 0.6 | 357.5 ± 42.7 | 2.3 ± 0.1 |
| 26 | 0.6 ± 0.0 | 0.11 ± 0.01 | 0.06 ± 0.00 | 16.2 ± 2.5 | 358.9 ± 15.8 | 2.3 ± 0.2 |
| 27 | **0.4 ± 0.0** | 0.07 ± 0.00 | 0.06 ± 0.00 | 20.1 ± 0.6 | 358.7 ± 92.8 | 2.9 ± 0.2 |

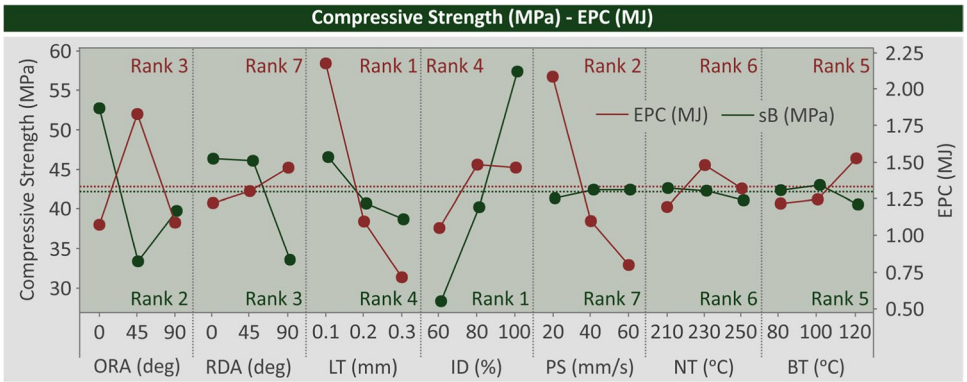


**Fig. 6** MEP of compressive strength (MPa) and energy (MJ) for the different control parameters

improved mechanical properties. Additionally, additives can further improve and reinforce the mechanical properties of the 3D-printed parts [15]. Such an investigation was outside the scope of the work.

Two works related to the optimization of the mechanical properties of 3D-printed parts made of ABS [10] and PLA [82] follow a similar approach to the current work but with fewer control parameters. Also, different types of mechanical properties were studied. A parameter that was not considered in these previous works was the ORA. This parameter was proven critical in the current study, showing the need for additional 3D printing setting evaluation as it is not obvious which parameter might affect the response metrics. Regarding the compressive strength of ABS parts in MEX 3D printing, different studies have been conducted, but none is studying so many parameters at the same time or employed modeling tools for the analysis of the experimental results [83–87]. Still, the compressive strength results

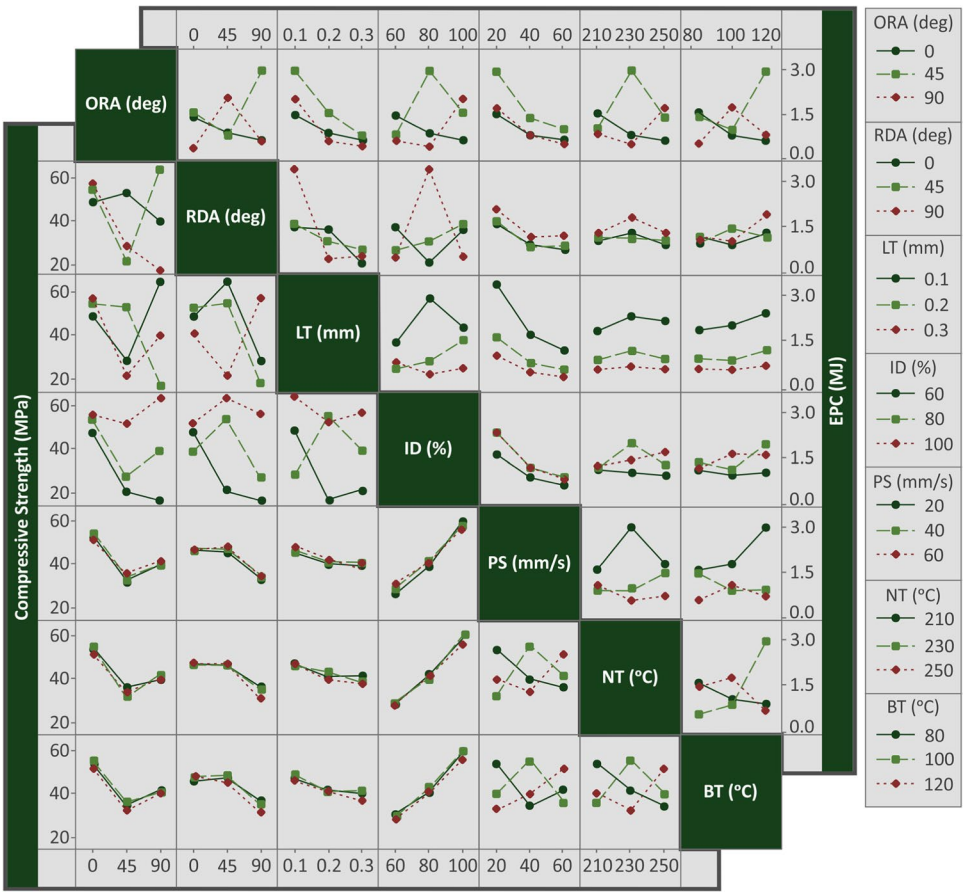


**Fig. 7** Interaction plots of compressive strength (MPa) and energy (MJ) for the different control parameters

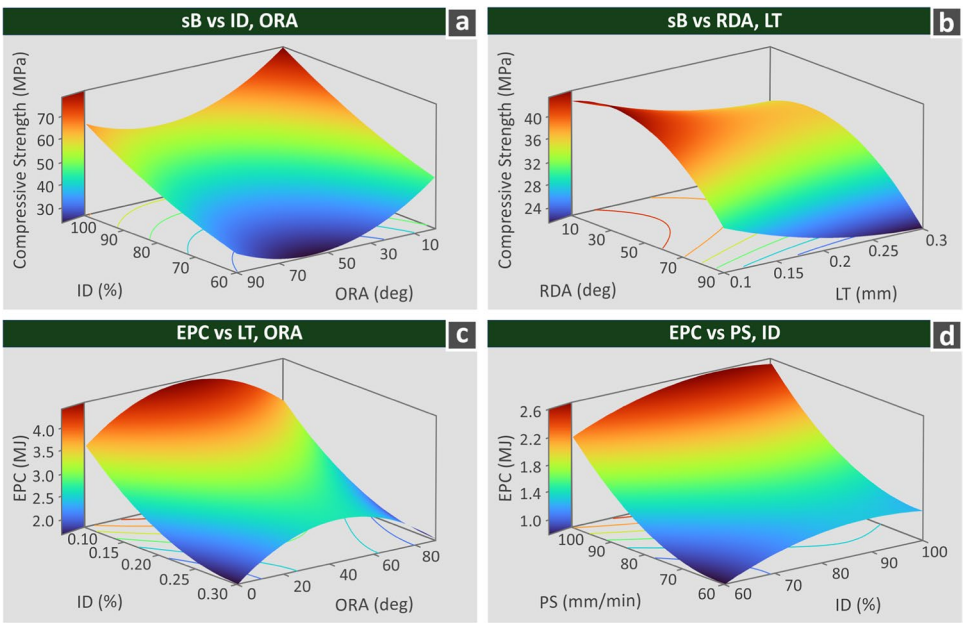


**Fig. 8** Surface graphs of compressive strength (MPa) and energy (MJ) for the different control parameters

are comparable and summarized in the following Table 3. Any differences can be attributed to the different ABS grades used, the experimental conditions, and mainly to the different 3D printing settings used and the lack of optimization in the existing studies. This highlights the importance of selecting appropriate 3D printing settings as their effect on

**Table 3** Experimental results of the current study in comparison to the literature

| Study | Material | Compressive strength (MPa) | Energy consumption (MJ) | 3D printing settings studied |
|---|---|---|---|---|
| Current | ABS | 14.00–65.30 | 0.400–2.400 | ORA, RDA, LT, ID, PS, NT, and BT |
| Lee et al. [85] | ABS | 41.26 | - | RDA |
| Yadav et al. [86] | ABS | 21.15 | - | RDA and infill pattern |
| Ahn et al. [83] | ABS | 40.00 | - | Bead width, ID, NT, RDA, and color |
| Ashtankar et al. [87] | ABS | 26.66 | - | RDA |
| Morocho et al. [84] | ABS | 33.15 | - | Infill pattern |
| Vidakis et al. [10] | ABS | - | 0.072–0.828 | RDA, LT, ID, PS, NT, and BT |
| Vidakis et al. [67] | PC | 67.08 | 0.32–5.130 | ORA, RDA, LT, ID, PS, NT, and BT |

the mechanical properties was here verified as well. It also highlights the need for optimization due to the wide range of the reported values herein and in the literature. The current study investigates more 3D printing parameters (seven) than similar works in the literature; at the same time, it reports higher compressive strength values than the existing literature. Therefore, it could be assumed that increasing the number of 3D printing parameters that are optimized leads to a more improved performance from the built parts.

Regarding energy consumption, the increase in the LT reduces the required energy for the 3D printing of the parts to 50% of the energy required at lower LT values. A similar outcome was found with the increase of the PS, which reduces the energy required to about 55% of the energy required at lower PS values. Such outcomes are indicating the importance of the 3D printing parameters in energy consumption as well. It should also be noted that the increase in the temperature parameters (NT and BT) does not significantly affect both the energy consumption and the compressive strength. On the other hand, energy consumption was found to be hugely affected by the printing time, which was also a response indicator in the study. The MEP pattern of the two response indicators is almost the same, showing a direct connection between the two metrics. In a work studying the energy consumption of ABS parts built with the MEX process, LT and PS were also the dominant parameters affecting the energy consumption, same as in the findings of the current work (higher values decreased EPC) [10]. A similar finding is also reported for the energy consumption of PC parts made with the MEX 3D printing process [67].

In the study, the Taguchi plan was followed. Different modeling tools could have been implemented, and there are several other prospect modeling methods. Herein, it was preferred to use this approach since two different research areas were investigated, i.e., energy consumption and the mechanical properties of the MEX ABS 3D-printed parts under compression loading. The analysis showed that each different area suggested a different set of significant parameters. If only the mechanical properties were investigated, approaches such as the fractional factorial plan would probably be more suitable. But it was required to have a comparable experimental effort in an attempt to optimize both research areas simultaneously with a common set of parameters if this was feasible. The fractional factorial plan would require two different and independent sets of experiments and two different optimization efforts. The number of levels was selected to be three, as a large number of experiments were already conducted in this experimental effort for the specific study.

## 5 Conclusions

This work provided inclusive and comprehensive results on the behavior under compressive loading of ABS MEX 3DP parts. For the time being, seven 3DP parameters are investigated for the effect on both the compressive properties of the parts and the energy consumed for their fabrication. An insight into the significance of each 3DP parameter is provided through the statistical analysis followed. LT and PS were the dominant parameters regarding the EPC, while NT and RDA were the least important settings. For the compression strength, ID and ORA were the dominant parameters and PS and NT were the least important parameters. Regarding the cons of the work, the experimental results presented are not generic for every polymer. Each polymer has different thermomechanical properties, different strand fusion mechanisms, etc., so corresponding processes are required for each polymer. The experimental data provided can be processed with various modeling tools such as artificial neural networks, among others, as future work. Additionally, although a large number of seven 3D printing parameters have been ranked and analyzed in the work for their statistical importance, the experimental process can be further expanded with additional parameters and levels to extend the applicability of the current research results.

**Supplementary Information** The online version contains supplementary material available at https://doi.org/10.1007/s00170-023-11202-w.

**Acknowledgements** The authors would like to thank Aleka Manousaki from the Institute of Electronic Structure and Laser of the Foundation for Research and Technology, Hellas (IESL-FORTH) for taking the SEM images presented in this work.

**Author contribution** Conceptualization: NV; methodology: NV; formal analysis and investigation: NM and AM, data curation: NM; writing (original draft preparation): MP; writing (review and editing): MP, funding acquisition: NV; resources: NV; supervision: NV. All authors have read and agreed to the published version of the manuscript.

**Funding** Open access funding provided by HEAL-Link Greece.

**Data availability** The raw/processed data required to reproduce these findings cannot be shared at this time due to technical or time limitations.

## Declarations

**Competing interests** The authors declare no competing interests.



## References

1. Wang X, Xu T, de Andrade MJ et al (2021) The interfacial shear strength of carbon nanotube sheet modified carbon fiber composites BT - challenges in mechanics of time dependent materials, volume 2. In: Silberstein M, Amirkhizi A (eds). Springer International Publishing, Cham, pp 25–32
2. Cao D, Malakooti S, Kulkarni VN et al (2021) Nanoindentation measurement of core–skin interphase viscoelastic properties in a sandwich glass composite. Mech Time-Depend Mater 25:353–363. https://doi.org/10.1007/s11043-020-09448-y
3. Cao D, Malakooti S, Kulkarni VN et al (2022) The effect of resin uptake on the flexural properties of compression molded sandwich composites. Wind Energy 25:71–93. https://doi.org/10.1002/we.2661
4. Vidakis N, Petousis M, Velidakis E et al (2023) Multi-functional medical grade polyamide 12/carbon black nanocomposites in material extrusion 3D printing. Compos Struct 116788. https://doi.org/10.1016/j.compstruct.2023.116788
5. Al-Saleh MH, Sundararaj U (2012) Microstructure, electrical, and electromagnetic interference shielding properties of carbon nanotube/acrylonitrile–butadiene–styrene nanocomposites. J Polym Sci Part B Polym Phys August 201:1356–1362. https://doi.org/10.1002/polb.23129
6. Díez-Pascual AM, Gascón D (2013) Carbon nanotube buckypaper reinforced acrylonitrile-butadiene-styrene composites for electronic applications. ACS Appl Mater Interfaces 5:12107–12119. https://doi.org/10.1021/am4039739
7. Moore JD (1973) Acrylonitrile-butadiene-styrene (ABS) - a review. Composites 4:118–130. https://doi.org/10.1016/0010-4361(73)90585-5
8. Kamelian FS, Saljoughi E, ShojaeeNasirabadi P, Mousavi SM (2018) Modifications and research potentials of acrylonitrile/butadiene/styrene (ABS) membranes: a review. Polym Compos 39:2835–2846. https://doi.org/10.1002/pc.24276
9. Nabi G, Malik N, Tahir MB et al (2021) Synthesis of graphitic carbon nitride and industrial applications as tensile strength reinforcement agent in red acrylonitrile-butadiene-styrene (ABS). Phys B Condens Matter 602:412556. https://doi.org/10.1016/j.physb.2020.412556
10. Vidakis N, Kechagias JD, Petousis M et al (2022) The effects of FFF 3D printing parameters on energy consumption. Mater Manuf Process 00:1–18. https://doi.org/10.1080/10426914.2022.2105882
11. Srinivasan Ganesh Iyer S, Keles O (2022) Effect of raster angle on mechanical properties of 3D printed short carbon fiber reinforced acrylonitrile butadiene styrene. Compos Commun 32:101163. https://doi.org/10.1016/j.coco.2022.101163
12. Bin Hamzah HH, Keattch O, Covill D, Patel BA (2018) The effects of printing orientation on the electrochemical behaviour of 3D printed acrylonitrile butadiene styrene (ABS)/carbon black electrodes. Sci Rep 8:1–8. https://doi.org/10.1038/s41598-018-27188-5
13. Huang B, He H, Meng S, Jia Y (2019) Optimizing 3D printing performance of acrylonitrile-butadiene-styrene composites. pdf. Soc Chem Ind 68:1351–1360. https://doi.org/10.1002/pi.5824
14. Kumar M, Ramakrishnan R, Omarbekova A (2019) 3D printed polycarbonate reinforced acrylonitrile–butadiene–styrene composites: composition effects on mechanical properties, microstructure and void formation study. J Mech Sci Technol 33:5219–5226. https://doi.org/10.1007/s12206-019-1011-9
15. Vidakis N, Petousis M, Maniadi A, Liebscher M, Tzounis L (2021) Mechanical properties of 3D-printed acrylonitrile–butadiene–styrene TiO2 and ATO nanocomposites. Polymers (Basel) 13:123–129. https://doi.org/10.3390/polym12071589
16. Vidakis N, Petousis M, Maniadi A et al (2020) The mechanical and physical properties of 3D-printed materials composed of ABS-ZnO nanocomposites and ABS-ZnO microcomposites. Micromachines 11:1–20. https://doi.org/10.3390/mi11060615
17. Vidakis N, Maniadi A, Petousis M et al (2020) Mechanical and electrical properties investigation of 3D-printed acrylonitrile–butadiene–styrene graphene and carbon nanocomposites. J Mater Eng Perform 29:1909–1918. https://doi.org/10.1007/s11665-020-04689-x
18. N J, P S (2019) Application of 3D printed ABS based conductive carbon black composite sensor in void fraction measurement. Compos B Eng 159:224–230. https://doi.org/10.1016/j.compositesb.2018.09.097
19. Harshit KD, Dixit US, Nedelcu D (2021) Recent advances in manufacturing processes and systems. Springer, Singapore. https://doi.org/10.1007/978-981-16-7787-8
20. Savvakis K, Petousis M, Vairis A et al (2014) Experimental determination of the tensile strength of fused deposition modeling parts. In: ASME International Mechanical Engineering Congress and Exposition, Proceedings (IMECE). ASME International, Montreal, Quebec, Canada
21. Ramezani Dana H, Barbe F, Delbreilh L et al (2019) Polymer additive manufacturing of ABS structure: Influence of printing direction on mechanical properties. J Manuf Process 44:288–298. https://doi.org/10.1016/j.jmapro.2019.06.015
22. Dhinesh SK, Arun PS, Senthil KKL, Megalingam A (2021) Study on flexural and tensile behavior of PLA, ABS and PLA-ABS materials. Mater Today Proc 45:1175–1180. https://doi.org/10.1016/j.matpr.2020.03.546

23. Raney K, Lani E, Kalla DK (2017) Experimental characterization of the tensile strength of ABS parts manufactured by fused deposition modeling process. Mater Today Proc 4:7956–7961. https://doi.org/10.1016/j.matpr.2017.07.132
24. Gordelier TJ, Thies PR, Turner L, Johanning L (2019) Optimising the FDM additive manufacturing process to achieve maximum tensile strength: a state-of-the-art review. Rapid Prototyp J 25:953–971. https://doi.org/10.1108/RPJ-07-2018-0183
25. Srinivasan R, Pridhar T, Ramprasath LS et al (2020) Prediction of tensile strength in FDM printed ABS parts using response surface methodology (RSM). Mater Today Proc 27:1827–1832. https://doi.org/10.1016/j.matpr.2020.03.788
26. Rosenthal Y, Stern A, Treivish I, Ashkenazi D (2019) Crack propagation in flexural testing of additive manufactured acrylonitrile butadiene styrene. Ann "Dunarea Jos" Univ Galati Fascicle XII, Weld Equip Technol 30. https://doi.org/10.35219/awet.2019.03
27. Travieso-Rodriguez JA, Jerez-Mesa R, Llumà J et al (2021) Comparative study of the flexural properties of ABS, PLA and a PLA–wood composite manufactured through fused filament fabrication. Rapid Prototyp J 27:81–92. https://doi.org/10.1108/RPJ-01-2020-0022
28. Mohamed OA, Masood SH, Bhowmik JL (2017) Investigation on the flexural creep stiffness behavior of PC–ABS material processed by fused deposition modeling using response surface definitive screening design. JOM 69:498–505. https://doi.org/10.1007/s11837-016-2228-z
29. Zhang H, Cai L, Golub M et al (2018) Tensile, creep, and fatigue behaviors of 3D-printed acrylonitrile butadiene styrene. J Mater Eng Perform 27:57–62. https://doi.org/10.1007/s11665-017-2961-7
30. Frascio M, Avalle M, Monti M (2018) Fatigue strength of plastics components made in additive manufacturing: first experimental results. Procedia Struct Integr 12:32–43. https://doi.org/10.1016/j.prostr.2018.11.109
31. Sadegh M, Parast A, Bagheri A et al (2022) Bending fatigue behavior of fused filament fabrication 3D - printed ABS and PLA joints with rotary friction welding. Prog Addit Manuf. https://doi.org/10.1007/s40964-022-00307-5
32. Jap NSF, Pearce GM, Hellier AK et al (2019) The effect of raster orientation on the static and fatigue properties of filament deposited ABS polymer. Int J Fatigue 124:328–337. https://doi.org/10.1016/j.ijfatigue.2019.02.042
33. Azadi M, Dadashi A, Dezianian S et al (2021) High-cycle bending fatigue properties of additive-manufactured ABS and PLA polymers fabricated by fused deposition modeling 3D-printing. Forces Mech 3:100016. https://doi.org/10.1016/j.finmec.2021.100016
34. Owolabi G, Peterson A, Habtour E et al (2016) Dynamic response of acrylonitrile butadiene styrene under impact loading. Int J Mech Mater Eng 11. https://doi.org/10.1186/s40712-016-0056-0
35. Alshammari YLA, He F, Khan MA (2021) Modelling and investigation of crack growth for 3D-printed acrylonitrile butadiene styrene (Abs) with various printing parameters and ambient temperatures. Polymers (Basel) 13. https://doi.org/10.3390/polym13213737
36. Vidakis N, Petousis M, Vairis A et al (2019) A parametric determination of bending and Charpy's impact strength of ABS and ABS-plus fused deposition modeling specimens. Prog Addit Manuf 4:323–330. https://doi.org/10.1007/s40964-019-00092-8
37. Hadidi H, Mailand B, Sundermann T et al (2019) Low velocity impact of ABS after shot peening predefined layers during additive manufacturing. Procedia Manuf 34:594–602. https://doi.org/10.1016/j.promfg.2019.06.169
38. Górski F, Kuczko W, Wichniarek R (2014) Impact strength of ABS parts manufactured using fused deposition modeling technology. Arch Mech Technol Autom 34(3–12)
39. Roberson DA, Torrado Perez AR, Shemelya CM et al (2015) Comparison of stress concentrator fabrication for 3D printed polymeric izod impact test specimens. Addit Manuf 7:1–11. https://doi.org/10.1016/j.addma.2015.05.002
40. Vairis A, Petousis M, Vidakis N, Savvakis K (2016) On the Strain rate sensitivity of ABS and ABS plus fused deposition modeling parts. J Mater Eng Perform 25:3558–3565. https://doi.org/10.1007/s11665-016-2198-x
41. Vidakis N, Petousis M, Velidakis E et al (2020) On the strain rate sensitivity of fused filament fabrication (Fff) processed PLA, ABS, PETG, PA6, AND PP thermoplastic polymers. Polymers (Basel) 12:1–15. https://doi.org/10.3390/polym12122924
42. Vidakis N, David CN, Petousis M et al (2022) Optimization of key quality indicators in material extrusion 3D printing of acrylonitrile butadiene styrene: The impact of critical process control parameters on the surface roughness, dimensional accuracy, and porosity. Mater Today Commun 34:105171. https://doi.org/10.1016/j.mtcomm.2022.105171
43. Kechagias J, Chaidas D, Vidakis N et al (2022) Key parameters controlling surface quality and dimensional accuracy: a critical review of FFF process. Mater Manuf Process 37:963–984. https://doi.org/10.1080/10426914.2022.2032144
44. Jayanth N, Senthil P, Prakash C (2018) Effect of chemical treatment on tensile strength and surface roughness of 3D-printed ABS using the FDM process. Virtual Phys Prototyp 13:155–163. https://doi.org/10.1080/17452759.2018.1449565
45. Pramanik D, Mandal A, Kuar AS (2020) An experimental investigation on improvement of surface roughness of ABS on fused deposition modelling process. Mater Today Proc 26:860–863. https://doi.org/10.1016/j.matpr.2020.01.054
46. Khan MS, Mishra SB (2020) Minimizing surface roughness of ABS-FDM build parts: an experimental approach. Mater Today Proc 26:1557–1566. https://doi.org/10.1016/j.matpr.2020.02.320
47. Vidakis N, Petousis M, Maniadi A et al (2020) Sustainable additive manufacturing: mechanical response of acrylonitrile-butadiene-styrene over multiple recycling processes. Sustain 12:3568. https://doi.org/10.3390/su12093568
48. Mohammed MI, Wilson D, Gomez-Kervin E et al (2019) Investigation of closed-loop manufacturing with acrylonitrile butadiene styrene over multiple generations using additive manufacturing. ACS Sustain Chem Eng 7:13955–13969. https://doi.org/10.1021/acssuschemeng.9b02368
49. Mohammed M, Wilson D, Gomez-Kervin E et al (2022) Sustainability and feasibility assessment of distributed E-waste recycling using additive manufacturing in a bi-continental context. Addit Manuf 50:102548. https://doi.org/10.1016/j.addma.2021.102548
50. Shanmugam V, Das O, Neisiany RE et al (2020) Polymer recycling in additive manufacturing: an opportunity for the circular economy. Mater Circ Econ 2:11. https://doi.org/10.1007/s42824-020-00012-0
51. Kechagias JD, Ninikas K, Petousis M, Vidakis N (2022) Laser cutting of 3D printed acrylonitrile butadiene styrene plates for dimensional and surface roughness optimization. Int J Adv Manuf Technol 119:2301–2315. https://doi.org/10.1007/s00170-021-08350-2
52. Gong K, Liu H, Huang C et al (2022) Hybrid manufacturing of acrylonitrile butadiene styrene (ABS) via the combination of material extrusion additive manufacturing and injection molding. Polymers (Basel) 14(23):5093. https://doi.org/10.3390/polym14235093
53. Hadidi H, Mailand B, Sundermann T et al (2020) Dynamic mechanical analysis of ABS from hybrid additive manufacturing by fused filament fabrication and shot peening. Proceedings of the ASME 2020 15th International Manufacturing Science and Engineering Conference vol 1: Additive Manufacturing; AdvancedMaterials Manufacturing; Biomanufacturing; Life Cycle Engineering; Manufacturing Equipment and Automation. Virtual, online. September 3, 2020. V001T01A047. ASME. https://doi.org/10.1115/MSEC2020-8253
54. Vidakis N, Petousis M, Korlos A et al (2022) Friction stir welding optimization of 3D-printed acrylonitrile butadiene styrene in hybrid additive manufacturing. Polymers (Basel) 14:2474. https://doi.org/10.3390/polym14122474
55. Hibbert K, Warner G, Brown C et al (2019) The effects of build parameters and strain rate on the mechanical properties of FDM

3D-printed acrylonitrile butadiene styrene. Open J Org Polym Mater 09:1–27. https://doi.org/10.4236/ojopm.2019.91001
56. Wu W, Geng P, Li G et al (2015) Influence of layer thickness and raster angle on the mechanical properties of 3D-printed PEEK and a comparative mechanical study between PEEK and ABS. Materials (Basel) 8:5834–5846. https://doi.org/10.3390/ma8095271
57. Mansour MT, Tsongas K, Tzetzis D (2021) 3D printed hierarchical honeycombs with carbon fiber and carbon nanotube reinforced acrylonitrile butadiene styrene. J Compos Sci 5. https://doi.org/10.3390/jcs5020062
58. Bhandari S, Lopez-Anido RA, Wang L, Gardner DJ (2020) Elasto-plastic finite element modeling of short carbon fiber reinforced 3D printed acrylonitrile butadiene styrene composites. Jom 72:475–484. https://doi.org/10.1007/s11837-019-03895-w
59. Morocho JR, Sánchez AC, Singaña M, Donoso C (2020) Effect of the filling pattern on the compression strength of 3D printed objects using acrylonitrile butadiene styrene (ABS). Key Eng Mater 834 KEM:115–119. https://doi.org/10.4028/www.scientific.net/KEM.834.115
60. Oudah S, Al-Attraqchi H, Nassir N (2022) The effect of process parameters on the compression property of acrylonitrile butadiene styrene produced by 3D printer. Eng Technol J 40:189–194. https://doi.org/10.30684/etj.v40i1.2118
61. Meraz Trejo E, Jimenez X, Billah KMM et al (2020) Compressive deformation analysis of large area pellet-fed material extrusion 3D printed parts in relation to in situ thermal imaging. Addit Manuf 33:101099. https://doi.org/10.1016/j.addma.2020.101099
62. Abdullah AM, Mohamad D, Rahim TNAT et al (2019) Effect of narrow infill density gap on the compressive properties of 3D printed carbon fibre reinforced acrylonitrile butadiene styrene. J Mech Sci Technol 33:2339–2343. https://doi.org/10.1007/s12206-019-0433-8
63. Domínguez-Rodríguez G, Ku-Herrera JJ, Hernández-Pérez A (2018) An assessment of the effect of printing orientation, density, and filler pattern on the compressive performance of 3D printed ABS structures by fuse deposition. Int J Adv Manuf Technol 95:1685–1695. https://doi.org/10.1007/s00170-017-1314-x
64. Uddin MS, Sidek MFR, Faizal MA et al (2017) Evaluating mechanical properties and failure mechanisms of fused deposition modeling acrylonitrile butadiene styrene parts. J Manuf Sci Eng Trans ASME 139:1–12. https://doi.org/10.1115/1.4036713
65. Dou H, Ye W, Zhang D et al (2022) Compression performance with different build orientation of fused filament fabrication polylactic acid, acrylonitrile butadiene styrene, and polyether ether ketone. J Mater Eng Perform 31:1925–1933. https://doi.org/10.1007/s11665-021-06363-2
66. Vidakis N, Petousis M, Konstantinos S et al (2015) Experimental determination of fused deposition modelling parts compressive strength. Int Conf New Horizons Ind Bus Educ Ski 93–98
67. Vidakis N, Petousis M, David CN et al (2023) Mechanical performance over energy expenditure in MEX 3D printing of polycarbonate : a multiparametric optimization with the aid of robust experimental design. J Manuf Mater Process 7:38. https://doi.org/10.3390/jmmp7010038
68. Chohan JS, Mittal N, Kumar R et al (2020) Mechanical strength enhancement of 3D printed acrylonitrile butadiene styrene polymer components using neural network optimization algorithm. Polymers (Basel) 12:1–18. https://doi.org/10.3390/polym12102250
69. Dev S, Srivastava R (2019) Experimental investigation and optimization of FDM process parameters for material and mechanical strength. Mater Today Proc 26:1995–1999. https://doi.org/10.1016/j.matpr.2020.02.435
70. Norani MNM, Bin AMF, Abdullah MIHC et al (2021) 3D printing parameters of acrylonitrile butadiene styrene polymer for friction and wear analysis using response surface methodology. Proc Inst Mech Eng Part J J Eng Tribol 235:468–477. https://doi.org/10.1177/1350650120925601
71. Vidakis N, Petousis M, Kechagias JD (2022) Parameter effects and process modelling of polyamide 12 3D-printed parts strength and toughness. Mater Manuf Process 37:1358–1369. https://doi.org/10.1080/10426914.2022.2030871
72. Kechagias JD, Vidakis N, Petousis M (2021) Parameter effects and process modeling of FFF-TPU mechanical response. Mater Manuf Process 38:341–351. https://doi.org/10.1080/10426914.2021.2001523
73. Annibaldi V, Rotilio M (2019) Energy consumption consideration of 3D printing. 2019 IEEE Int Work Metrol Ind 40 IoT, MetroInd 40 IoT 2019 - Proc 243–248. https://doi.org/10.1109/METROI4.2019.8792856
74. Peng T (2017) Energy modelling for FDM 3D printing from a life cycle perspective. Int J Manuf Res 11:1. https://doi.org/10.1504/ijmr.2017.10003722
75. El you El idrissi MA, Laaouina L, Jeghal A et al (2022) Energy consumption prediction for fused deposition modelling 3D printing using machine learning. Appl Syst Innov 5:1–16. https://doi.org/10.3390/asi5040086
76. Peng T (2016) Analysis of energy utilization in 3D printing processes. Procedia CIRP 40:62–67. https://doi.org/10.1016/j.procir.2016.01.055
77. De Bernardez L, Campana G, Mele M et al (2022) Effects of infill patterns on part performances and energy consumption in acrylonitrile butadiene styrene fused filament fabrication via industrial-grade machine. Prog Addit Manuf. https://doi.org/10.1007/s40964-022-00316-4
78. Colorado HA, Velásquez EIG, Monteiro SN (2020) Sustainability of additive manufacturing: the circular economy of materials and environmental perspectives. J Mater Res Technol 9:8221–8234. https://doi.org/10.1016/j.jmrt.2020.04.062
79. Khosravani MR, Reinicke T (2020) On the environmental impacts of 3D printing technology. Appl Mater Today 20:100689. https://doi.org/10.1016/j.apmt.2020.100689
80. Jung W-K, Kim H, Park Y-C et al (2020) Smart sewing work measurement system using IoT-based power monitoring device and approximation algorithm. Int J Prod Res 58:6202–6216. https://doi.org/10.1080/00207543.2019.1671629
81. Phadke MS (1995) Quality engineering using robust design, 1st edn. Prentice Hall PTR, USA
82. Kechagias JD, Vidakis N, Petousis M, Mountakis N (2022) A multiparametric process evaluation of the mechanical response of PLA in FFF 3D printing. Mater Manuf Process 00:1–13. https://doi.org/10.1080/10426914.2022.2089895
83. Ahn S, Montero M, Odell D et al (2002) Anisotropic material properties of fused deposition modeling ABS. Rapid Prototyp J 8:248–257. https://doi.org/10.1108/13552540210441166
84. Morocho JR, Sánchez AC, Singaña M, Donoso C (2020) Effect of the filling pattern on the compression strength of 3D printed objects using acrylonitrile butadiene styrene (ABS). Key Eng Mater 834:115–119. https://doi.org/10.4028/www.scientific.net/KEM.834.115
85. Lee CS, Kim SG, Kim HJ, Ahn SH (2007) Measurement of anisotropic compressive strength of rapid prototyping parts. J Mater Process Technol 187–188:627–630. https://doi.org/10.1016/j.jmatprotec.2006.11.095
86. Yadav DK, Srivastava R, Dev S (2020) Design & fabrication of ABS part by FDM for automobile application. Mater Today Proc 26:2089–2093. https://doi.org/10.1016/j.matpr.2020.02.451
87. Ashtankar KM, Kuthe AM, Rathour BS (2013) Effect of build orientation on mechanical properties of rapid prototyping (fused deposition modelling) made acrylonitrile butadiene styrene (ABS) parts. Proceedings of the ASME 2013 International Mechanical Engineering Congress and Exposition, volume 11: Emerging Technologies. San Diego, California, USA. V011T06A017. ASME. https://doi.org/10.1115/IMECE2013-63146